Simulation of an Adaptable Hall Thruster

IEPC-2019-838

Presented at the 36th International Electric Propulsion Conference
University of Vienna, Austria
September 15-20, 2019

Nicholas D. Proulx * and Manish Jugroot†
RAPPEL Lab, Royal Military College of Canada, Kingston, Ontario, K7K 7B4, Canada

With the range of maneuvers required by satellites constantly expanding and increasing in complexity, from orbit insertion to constellation maintenance, the requirement becomes clear that a thruster with a range of operational parameters, that can be changed in-situ, is valuable. It would allow for a broader range of mission requirements to be completed with the same thruster in either a more timely, or more propellant efficient manner. Technology is currently available to convert materials between conductive and insulative states. This occurs through the addition of a precursor into the propellant, at plasma densities and temperatures seen in Hall Effect Thrusters (HET). This allows for the conversion between SPT and TAL configurations. A preliminary investigation into the range of operating parameters that could be achieved using adaptable HETs was conducted. A simulation consisting of geometry based off the P5 SPT thruster was ran in a TAL configuration. A 2D3V PIC code was used, with a Vaughan model to predict secondary electron emission as a function of energy and incident angle. The code was modified to force the SEE yield curve to match experimental values of the SEE yield transition energy for stainless steel. The results of the simulation are compared against experimental data for the thruster in the SPT configuration.

*Graduate Student, Mechanical and Aerospace Engineering, nproulx@rmc.ca
†Department Head and Professor, Mechanical and Aerospace Engineering, jugroot-m@rmc.ca

Nomenclature

$2D3V$	two geometric and three velocity dimensions
A	area
B	magnetic field
δ	SEE yield coefficient
ϵ	energy of incident particle
η	efficiency
HET	Hall effect thruster
I_{sp}	specific impulse
$\dot{m}$	massflow
m	mass
n	number density
$np2c$	number of particles per computer particle
SEE	secondary electron emission
SPT	stationary plasma thruster
T_e	electron temperature
TAL	thruster with anode layer
θ	angle
u	bulk velocity
v	exhaust velocity

I. Introduction

Adaptive satellite thrusters have the potential to bridge the demands of efficiency vs timeliness on increasingly complex missions. Missions can involve deep space, or requirements for counteracting atmospheric drag, station keeping, deorbiting, attitude adjustment, and both orbit insertion and transfers[1]. The use of constellations and formation flight impose additional layers of complexity. Adaptive thrusters will allow in flight modification of the operational parameters such as thrust and specific impulse (I_{sp}) through modification of wall materials. This will allow a broader range of mission requirements to be performed in a more timely, or more propellant efficient manor.

HETs belong to the electrostatic class of electric propulsion. Typical geometry consist of an annular channel, with an anode upstream and an electron source downstream. To summarize the physics, electrons are accelerated upstream towards the anode, where they collide and ionize a gaseous propellant emitted by the anode. A radial magnetic field lowers electron mobility, trapping electrons at the channel exit, creating a potential which accelerates ions, generating thrust. Gridded ion thrusters are the main alternative to HETs, however they are subject to space charge effects and typically have lower thrust and higher I_{sp}.

HETs come in two varieties which are differentiated based on channel wall material, SPT and TAL, with the former being a dielectric and latter being conductive. An additional hybrid type, termed dual mode HETs have also been the subject of recent investigations[2]. SPT have been studied more extensively than TAL, however literature suggests increased I_{sp} is attainable with TAL configurations [3]. The channel wall material significantly affects the plasma through properties such as conductivity and the secondary electron emission, allowing a higher T_e to develop which in turn support larger electric fields[4]. This results in channel depths approximately 8 times shorter in TAL configurations, or around half the width of the channel[4−5]. This close proximity to the anode is one of the main factors which contribute to TALs performance, although deeper channel configurations have been demonstrated [5]. The ability to modify the channel wall properties in-situ may allow some of the variations seen in TAL to be realized in SPT configurations.

NASA's 2015 Nanotechnology Roadmap refers to nanotechnology as having the potential for implementation in electric thrusters [6]. The basis for this study is a preliminary investigation of the potential benefits of an adaptable thruster. This adaption can be realized through the utilization of nanotechnology to change wall conductivity and secondary electron emission, allowing adaptation from a stationary plasma thruster configuration, to a thruster with anode layer configuration. The transition of graphene (electrical conductor) to graphane (insulator) has been demonstrated in plasmas with temperatures and densities similar to the plasma's in HETs [7]. The addition of a precursor such as metal hydrides to the propellant could allow for the adaptation between SPT and TAL to occur during operation[8]. With graphene being the strongest material in nature, and carbon showing itself highly resilient against sputtering, channel wall erosion may also be reduced[8]. This paper contains the results of an initial investigation into the variation of thrust and I_{sp} due to altering wall properties while holding the thruster geometry constant, in an SPT optimized configuration.

II. Theory

A. Propellant efficiency *vs* maneuver completion

The Tsiolkovsky rocket equation (Eqn. 1) demonstrates that a higher exhaust velocity (v_{exh}) allows us to perform the same maneuver using less propellant mass. This must be considered with the relationship of v_{exh} to thrust. Equation 2 is the rearranged efficiency equation, and displays how for a given amount of power, an increase in v_{exh} relates to a decrease in thrust. The ability to vary I_{sp} allows timely completion of large Δv maneuvers such as orbit transfers, while providing propellant efficiency and smaller impulse bits for fine thrust requirements.

$$\Delta v = -v_{exh} ln \frac{m_0}{m_f} \tag{1}$$

$$P_{elec} = \frac{\dot{m}c^2}{2\eta} \tag{2}$$

B. Secondary electron emission

Plasma parameters are significantly effected by secondary electron emission. Parameters used to characterize SEE include SEE yield, onset energy, critical energy, max yield, and max yield energy. The SEE yield is a coefficient which provides the number of secondary electrons produced per incident particle, typically determined empirically. It is a function of the incident particles energy and angle, is determined empirically, and embodies incident electrons that are reflected off the wall, scattered electrons, and true secondary electrons. The critical energy occurs when the SEE yield transitions across 1. The onset energy is the minimum energy before secondary electrons begin being emitted and the SEE typically has a maximum emission value, which occurs at a the max yield energy.

As electrons are accelerated from the emitter to the anode, their energy increases until it reaches the critical energy. The result is the channel walls are divided into two axial regions where SEE yield coefficient less than 1 near the thruster exit, resulting in a negative charge buildup on the channel walls, repelling electrons [4]. As the electrons are accelerated further towards the anode, the energy increases, the SEE yield transitions to greater than 1, resulting in a positive charge build up on the walls. This positive charge attracts electrons, and quenches any further increase in electron temperature.

The point that this transition occurs is a function of the channel materials SEE. Materials with high δ such as insulators allow the transition from a electron repelling region to electron attracting region at a lower T_e [4]. This results in a lower global T_e, and lower gradients. Lower gradients require a longer acceleration channel, with dielectric channels requiring an acceleration channel approximately 7.8 times longer [4].

III. Modeling

The fluid equations are useful for modelling highly collisional flows, however challenges arise in their application to HET's due to the Knudson numbers involved. Kinetic theory can be applied to rarefied gases since it applies classical mechanics to every individual particle, allowing for highly accurate but computationally expensive results.

PIC is a kinetic method which uses super particles, a single "superparticle" represents a multitude of actual particles. The superparticles position and velocity is measured in a continuous domain, while the fields are located at discrete nodes. The initial conditions provide the super particles position and velocity, and are used to determine the charge density. The Poisson equation is then invoked to determine the electric potential. This field is interpolated from the discrete nodes to the superparticles location, and forces calculated. The forces update the velocity, and position is determined using the updated velocity and time step. Particles are then injected or removed at various boundaries, and collisions are determined through probability calculations. The algorithm is then restarted by calculating the charge densities. A summary of the algorithm can be seen in Figure 1.

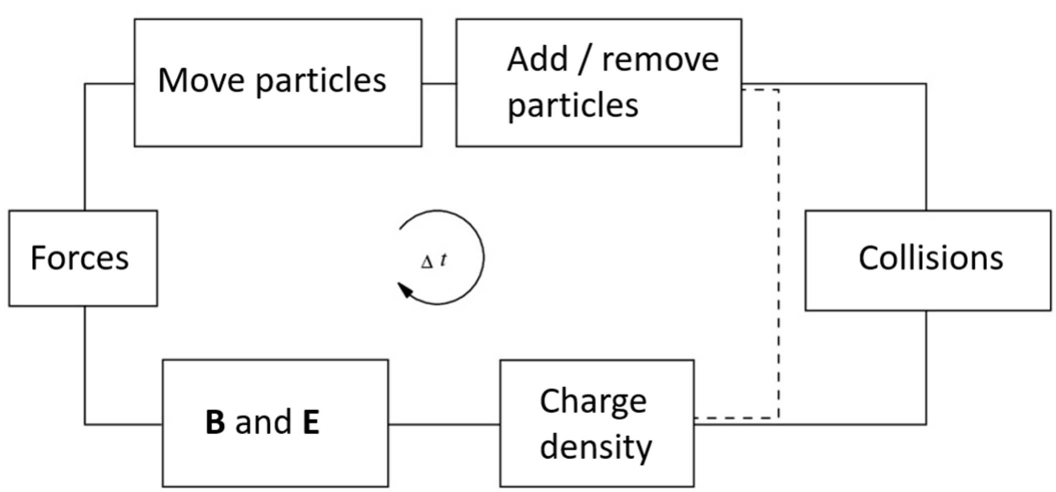

Figure 1: Xoopic particle in cell algorithm [9]

The software used is Xoopic, a general 2D3V PIC code[10]. It contains electrostatic and electromagnetic solvers, and utilizes a Boris Leapfrog advance for updating particle positions. It allows dielectric, and conductive boundary conditions and contains a Vaughan SEE model. The Vaughan based model is seen in Equation 3, and is a function of the incident electron energy (ϵ), and the particle angle of incidence (θ), the max yield coefficient (δ_*), and the associated incident energy (ϵ_*) [11]. Once the emission threshold (ϵ_0) for SEE is reached, the model is applied. It is worth noting that Equation 4 uses modified values to ensure δ transitions across 1 at the critical energy ϵ_1 for stainless steel.

$$\delta(\epsilon, \theta) = \delta_*(1 + k_{s\delta}\frac{\theta^2}{2\pi})(w\ exp(1-w))^k \tag{3}$$

$$k = \begin{bmatrix} 0.648\ w < 1 \\ 0.25\ w > 1 \end{bmatrix} \tag{4}$$

$$w = \frac{\epsilon - \epsilon_0}{\epsilon_*(1 + k_{sw}\theta^2/2\pi) - \epsilon_0} \tag{5}$$

IV. Method

As described above, Xoopic, an object oriented PIC code was selected over fluids equations due to the ability to implement account for anomalous electron transport with increased accuracy. Electron mobility across magnetic field lines, termed anomalous electron transport cannot be described by classical collisions. The result is increased current to the anode, due to instability driven azimuthal oscillations[12]. The geometry, magnetic, wall materials, neutral gas, electron injection and controls are summarized below.

A. Geometry

The base geometry is modeled after the P5 thruster[13−14]. The inner channel wall starts at 1.25cm, with a channel width of 2.5cm, and a height of 3.81 cm.

B. Magnetic Field

The magnetic field was modelled in Comsol Multiphysics, using the AC/DC module then input into the PIC code. Magnetic field was modelled after experimental results that contained the axial profile of the radial magnetic field strength at the inner wall, outer wall, and center. The reconstructed field was designed following the experimental values for the inner and center, and then mirrored. Figure 2 shows the field lines and strength, Figure 3 confirms that the axial distribution of the radial **B** field near the inner wall and the center of the channel match reasonably well with experimental values, with both peaking in the 170G-180G range.

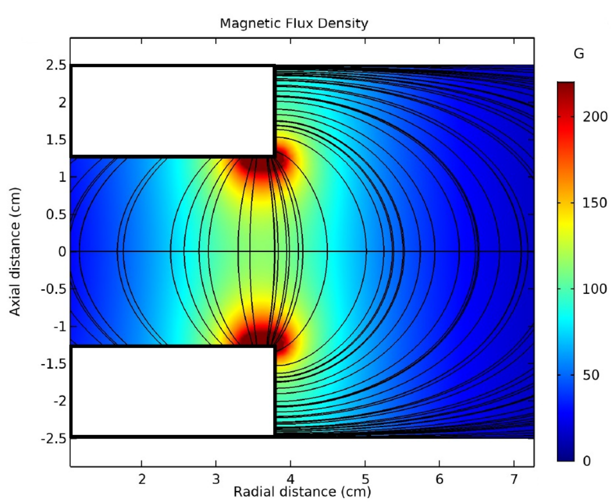

Figure 2: Simulated magnetic field matching P5 magnetic field

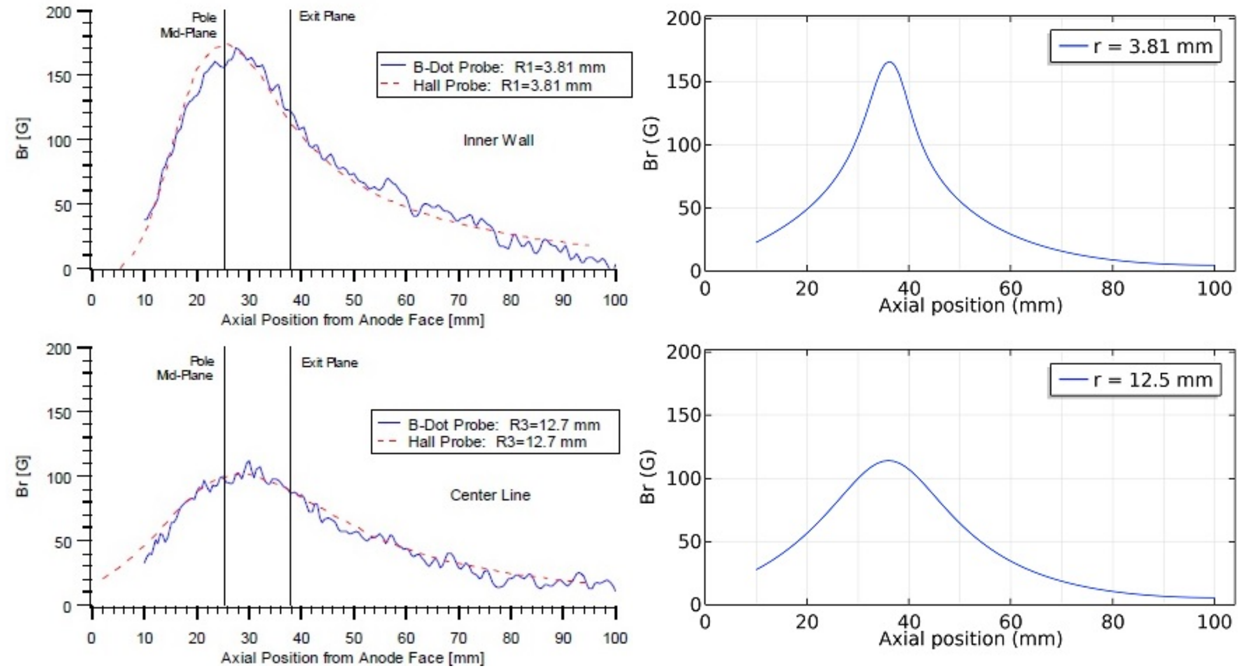

Figure 3: LHS: Experimentally measured P5 **B** field (from[14]). RHS: Simulated magnetic field in PIC

C. Wall Materials

The wall materials would ideally be selected as graphane and graphene, this is currently being investigated and will be presented in our future work. These present comparison involves the common materials BN-SiO_2 and stainless steel for the SPT and TAL configurations respectively. The parameters are summarized in Table 1. The transition temperature was calculated based based on Vaughan, and fit well with experimental results [11,15]. The emission temperature was based on stainless steels work function[15].

Table 1: SEE Coefficients[15−16]

Parameter	Value
δ_*	2.02
$\epsilon*$	200 eV
ϵ_1	46 eV
ϵ_0	4.4 eV

D. Neutral Gas

The neutral propellant gas was modelled as a static background density. This is acceptable due to the neutrals being unaffected by fields, and their trajectories linear[5]. The neutral density was estimated based on the 10.2 mg/s massflow used for the P5 thruster experimental data. Equation 6 was used to calculate the maximum density, while Figure 4 was used to determine the density profile [17]. The ionization fraction f_i was set to 0 directly at the anode, and a bulk velocity of 167 m/s was used[17].

$$n_n = (1 - f_i)\frac{\dot{m}/m_{Xe}}{A_C < u >} \tag{6}$$

An exponential decay was used to input the density profile into the simulation, $n_n \propto 3.35 \times e^{-22x1}; x = [0, 0.031]$, where x1 is the axial distance. This was derived from the general neutral decay profile of a 300V

10mg/s seen in Figure 4. The neutral density in the near field is neglected.

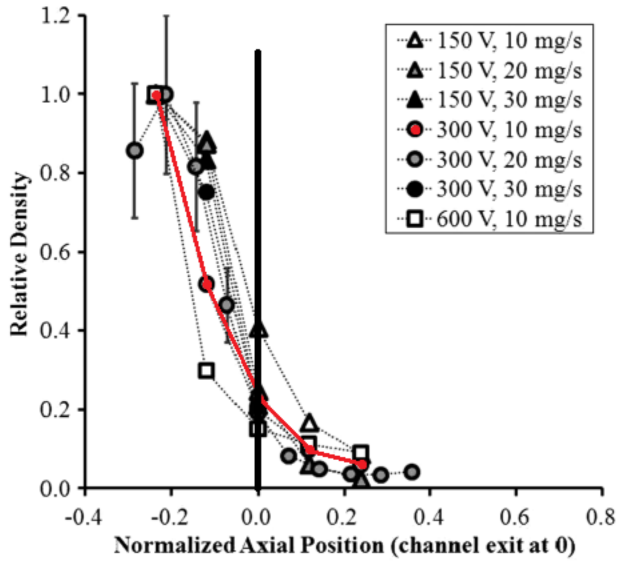

Figure 4: Neutral density profile of a 300V 10 mg/s Xe massflow (from[17])

E. Collisions

Collisions between the static neutral Xe, Xe^+ and e^- are accounted for by the MCC module. Events include ionization, excitation, and charge exchange. Secondary ionization is currently neglected. While charge exchange collisions are handled, the energized neutrals are not taken into account during thrust calculations.

F. Electron Injection

Electrons are injected along the axis of symmetry with a T_e of 10 eV. The ejection boundary is 1 cm long, starting 2 cm downstream of the thruster exit. The cathode starts at an initial value, after a delay it will ramp up to the final value. The initial current remains at .1A for the 1 μs, then ramps up to 5.4 A over the next 10 μs, where it then remains constant.

The grid and control parameters used for the simulation are shown in table 2.

Table 2: Model parameters and control

Parameter	**Value**
Axial grid length	9 cm
Radial grid length	5 cm
Axial cells	90
Radial cells	50
np2c	6x10^6
Timestep	$10^{-10}s$
Solve	electrostatic
ion subcycle	20
Scaling	none

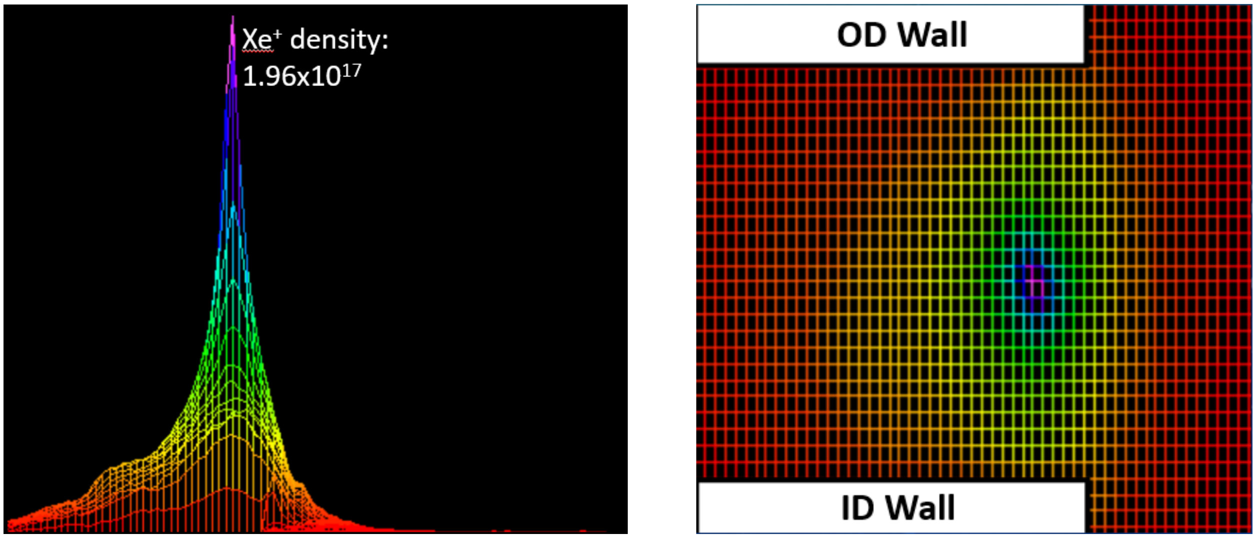

(a) Profile (b) Contour

Figure 5: Xe^+ number density peak

V. Results and Discussion

The results are taken from 30 μs to 32 μs, ion data was exported every 2×10^{-9} seconds, or every twenty steps and then averaged. Results can be seen in Table 3, and were taken 2 cm downstream, where the simulations electric field drops off and by this point it is estimated 99% of the thrust has been realized [13].

Table 3: Simulation results *vs* experimental measurements [13–14]

Parameter	TAL Simulation	Experimental
Thrust	7 mN	98 mN
I_{sp}	3400	1550s
I_d	5.4A	5.4A
V	300V	300V
n_i	.6-2 $\times 10^{17}$	2-6 $\times 10^{17}$
n_n	3.35×10^{19}	—
$\dot{m}_a$	—	10.2 mg/s
P background	0	6.6×10^{-6}
Channel material	SS	BN-SiO_2

The preliminary results are promising in terms of I_{sp}, however nothing conclusive can be established due to the fact that the comparison is between simulation and experimental values with different parameters. To increase confidence the implementation of an SPT version with a $BN - SiO_2$ would allow a more direct comparison, allowing both SPT and TAL configurations being under the same assumptions and neglections. Future work will include such an SPT model, as well as improved physical parameters, and optimized geometry.

Improvements to accuracy may be seen through the addition of secondary ionization, which can account for 23% of the discharge current in the plume of the P5 thruster[18]. Additionally modeling neutrals as particles will allow increased accuracy of neutral densities, as well as extension of neutral densities past the thruster exit[19]. Static background gas may still be employed, however its role will be in simulation of the background gas present in vacuum chambers during testing.

Closer modeling of the magnetic field in Comsol may provide additional accuracy. This may be realized through modeling both inner and outer chamber wall fields, as opposed to mirroring the inner wall. Attention may be given to matching the axial **B** field. Acquisition of the actual magnetic field data would enable much closer modeling of the field.

Further improvements can be seen by implementing electron effects such as accounting mobility, and temperature effects on SEE yield. An anomalous electron model such as the Bohm mobility model for $\mathbf{B}_\perp$ will account for the increased current seen in HETs which cannot be explained solely by classical collision. Finally the SEE coefficients for stainless steel were determined at room temperature conditions, whereas operation is at 500^{o}C. Studies on SEE on HET dielectrics have demonstrated a significant increase in SEE yield due to this increase in temperature[20]. Further research is required to determine if this is applicable to stainless steel as well.

VI. Conclusion

A TAL configuration thruster was simulated using PIC methods in a SPT geometry. A 7 mN thrust and 3400 s I_{sp} was estimated and compared against experimental values of 98 mN and 1550 s in the SPT P5 thruster. This simulation will be the basis for further study, including construction and characterization of a prototype that uses nanotechnology related solutions to perform adaptation between SPT and TAL configurations, and will be characterized using infrastructure in RAPPELs lab [21]. This will provide the foundation for further research where the application of the precursor to walls can potentially be used to increase wear resistance and potentially have self healing properties [8].

Acknowledgments

N. Proulx would like to acknowledge the support of the Natural Sciences and Engineering Research Council of Canada *NSERC (Discovery Grant)* and the Directorate General Space *DG Space (Canada).*

References

[1] Krejci, D., and Lozano, P., Space Propulsion Technology for Small Spacecraft, Proceedings of the IEEE, Vol. 106, No. 3,2018, pp. 362378.

[2] A. Christou and M. Jugroot, ”Investigating a two-stage electric space propulsion system: Simulation of plasma dynamics”, Vacuum, vol. 141, pp. 22-31, 2017.

[3] Reading, C.M.M and Frisbee, R. ”Very High Isp Thruster with Anode Layer (VHITAL) An Overview” AIAA 2004-5910.

[4] Choueiri, E. (2001). Fundamental difference between the two Hall thruster variants. Physics of Plasmas, 8(11), pp.5025-5033.

[5] Goebel, D. and Katz, I. (2008). Fundamentals of electric propulsion. Hoboken, NJ: Wiley.

[6] NASA Technology Roadmaps TA 10: Nanotechnology, Jul. 2015.

[7] Ryu, S., Han, M., Maultzsch, J., Heinz, T., Kim, P., Steigerwald, M. and Brus, L. (2008). Reversible Basal Plane Hydrogenation of Graphene. Nano Letters, 8(12), pp.4597-4602.

[8] Levchenko, I., Xu, S., Teel, G., Mariotti, D., Walker, M. L. R., and Keidar, M., Recent progress and perspectives of space electric propulsion systems based on smart nanomaterials, Nature Communications, Vol. 9, No. 1, 2018.

[9] Verboncoeur, J. (2005). Particle simulation of plasmas: review and advances. Plasma Physics and Controlled Fusion, 47(5A), pp.A231-A260.

[10] J.P. Verboncoeur, A.B. Langdon and N.T. Gladd, ”An Object-Oriented Electromagnetic PIC Code”, Comp. Phys. Comm., 87, May11, 1995, pp. 199-211

[11] Vaughan, J. (1989). A new formula for secondary emission yield. IEEE Transactions on Electron Devices, 36(9), pp.1963-1967.

[12] Lafleur, T., Baalrud, S. and Chabert, P. (2016). Theory for the anomalous electron transport in Hall effect thrusters. II. Kinetic model. Physics of Plasmas, 23(5), p.053503.

[13] Haas, J. (2001). ”Low-Perturbation Interrogation of the Internal and Near-Field Plasma Structure of A Hall Thruster Using A High-Speed Probe Positioning System” Ph.D. University of Michigan.

[14] Peterson, P., Gallimore, A. and Haas, J. (2002). ”An experimental investigation of the internal magnetic field topography of an operating Hall thruster.” Physics of Plasmas, 9(10), pp.4354-4362.

[15] Joy, D.C. "A Database of Electron Solid Interactions" University of Tennessee

[16] El-Nadi, L. (2013). Modern Trends in Physics. World Scientific Publishing Company, Singapore p.P.190.

[17] Huang, W., Gallimore, A. and Hofer, R. (2011). Neutral Flow Evolution in a Six-Kilowatt Hall Thruster. Journal of Propulsion and Power, 27(3), pp.553-563.

[18] Gulczinski, F.S., Examination of the Structure and Evolution of Ion Energy Properties of a 5 kW Class Laboratory Hall Effect Thruster at Various Operational Conditions, Ph.D. Thesis, University of Michigan Department of Aerospace Engineering, 1999.

[19] Jugroot, M., Harvey, J.K., "Numerical Modeling of Neutral and Charged Particles within a Gridded Ion Thruster," IEPC-01-100, Sept. 2001.

[20] M. Belhaj, K. Guerch, P. Sarrailh and N. Arcis, "Temperature effect on the electron emission and charging of BNSiO2 under low energy electron irradiation", Nuclear Instruments and Methods in Physics Research Section B: Beam Interactions with Materials and Atoms, vol. 362, pp. 163-166, 2015.

[21] B. Little and M. Jugroot, "Development of a microthrust balance and ion beam measurement system: Characterizing a dual-mode thruster for spacecraft", Vacuum, vol. 164, pp. 367-380, 2019.